Available online at www.sciencedirect.com

ScienceDirect

Materials Research Bulletin 43 (2008) 1263–1275

Materials Research Bulletin

www.elsevier.com/locate/matresbu

Thermal and mechanically activated decomposition of $LiAlH_4$

J.R. Ares [a,*], K.-F. Aguey-Zinsou [b], M. Porcu [a], J.M. Sykes [a],
M. Dornheim [b], T. Klassen [b], R. Bormann [b]

[a] *Department of Materials, Oxford University, Parks Road OX1 3PH, Oxford, UK*
[b] *Institute for Materials Research, GKSS-Forschungszentrum, Max-Planck-Str. 1, D-21502 Geesthacht, Germany*

Received 4 May 2006; received in revised form 13 February 2007; accepted 20 May 2007

Abstract

Thermal stability of as-received $LiAlH_4$ and milled $LiAlH_4$ has been investigated. The thermal decomposition mechanism of as-received $LiAlH_4$ depends on the temperature–time history. Apparent activation energies and enthalpies of the reactions have been obtained. During milling treatment, the high temperature and pressures locally induced by shocks lead to $LiAlH_4$ mechanically decomposition. The decomposition temperatures of $LiAlH_4$ and Li_3AlH_6 are both reduced by $\sim$60 °C due to particle size reduction produced by mechanical milling. Besides, the activation energy of the decomposition reaction of $LiAlH_4$ decreases as compared to as-received $LiAlH_4$. Moreover, a layer of oxide ($\sim$5 nm) at the surface of the milled alanate Li_3AlH_6 is observed. This layer could have a drastic influence on decomposition H-kinetics.

Keywords: A. Hydrides; C. Differential scanning calorimetry; C. Electron microscopy; D. Energy storage

---

1. Introduction

During the last 20 years, interest on hydrogen as a fuel for vehicles has increased substantially. One of the main tasks to be fulfilled is to develop a suitable on board H-storage system. On board H-storage systems need to be safe, low cost, with high gravimetric hydrogen capacity and rapid hydrogen absorption/desorption kinetics at ambient temperature and atmospheric pressures. At present, several storage materials are being investigated [1–3] and, among them, complex hydrides containing a AlH_4^- group (alanates) seem to be the most promising candidates due to their high gravimetric hydrogen capacity. In spite of this, alanates were not considered as candidates for H-storage until Bogdanovic and Schwickardi in 1997 demonstrated hydrogen reversibility under moderate pressures by adding $TiCl_3$ to sodium alanate [3]. After this work, investigations focused on improving the H-properties of sodium alanate by mechanically milling $NaAlH_4$ with different additives [4–6] have been done.

The progresses made with $NaAlH_4$ have led to consider it as a model-system for other alanates with higher H-capacity (10.6 wt%), such as $LiAlH_4$. $LiAlH_4$ was synthesised in the late 1940s and is usually used as a reducing agent. Only few groups explored the structural [7] and thermal properties [8–10] of $LiAlH_4$ until 10 years ago. But, since the discovery of the reversibility with $NaAlH_4$, investigations with $LiAlH_4$ as a potential H-storage material have

---

* Corresponding author. Present address: Laboratorio de Materiales de Interés Energético. Dpto. Física de Materiales. Facultad de Ciencias C-IV. UAM. 28049. Madrid (Spain). Tel.: +34 91497477; fax: +34 914978579.
E-mail address: joser.ares@uam.es (J.R. Ares).

0025-5408/$ – see front matter © 2007 Elsevier Ltd. All rights reserved.
doi:10.1016/j.materresbull.2007.05.018

greatly increased. Hydrogen desorption kinetics has been improved by milling $LiAlH_4$ with additives [11–15] and some degree of reversibility (1.8 wt%) was achieved by Chen et al. [15]. However, at present, the mechanism of absorption/desorption of hydrogen and the role of additives are not well understood.

The first step to understand the possible catalytic role of the additives during desorption of hydrogen in $LiAlH_4$ should be investigate the decomposition mechanism of $LiAlH_4$. As in all alkaline-alanates [16], the thermal decomposition of $LiAlH_4$ is summarised in the following two-step process:

$$LiAlH_4 \rightarrow \tfrac{1}{3}Li_3AlH_6 + \tfrac{2}{3}Al + H_2\ (5.3\,\mathrm{wt\%\,H}) \quad (T = 150 - 175\,^{\circ}\mathrm{C}) \quad \text{Reaction I} \tag{1}$$

$$\tfrac{1}{3}Li_3AlH_6 \rightarrow LiH + \tfrac{1}{3}Al + \tfrac{1}{2}H_2\ (2.6\,\mathrm{wt\%\,H}) \quad (T = 180 - 220\,^{\circ}\mathrm{C}) \quad \text{Reaction II} \tag{2}$$

However, this reaction route is more complex when it is analysed carefully. For instance, whereas a mechanism in which $LiAlH_4$ melts before it is decomposed into Li_3AlH_6 has been suggested by Dymova et al. [17] and supported by DTA, TG and DSC measurements [10,17], the decomposition of $LiAlH_4$ at temperatures lower than the melting point has been detected by ‘‘in situ’’ XRD and NMR [18,19].

In order to explain these results, the existence of intermediate reactions in (1) and (2) have been proposed. Wiench et al. [19] suggest that $LiAlH_4$(s) decomposes directly into LiH(s) and Al(s) expelling hydrogen, and that LiH(s) recombines with $LiAlH_4$(s) to produce Li_3AlH_6. Both reactions are thermodynamically feasible ($\Delta G^{\circ}_{r} < 0$) [20], and, for instance, recombination of LiH(s) with $LiAlH_4$(s) to obtain Li_3AlH_6(s) is often made by mechanical milling [11,20]. However, as far as we know, LiH(s) has never been detected. This situation might be explained by the very fast kinetics of the recombination reaction, which implies that detection of LiH(s) could be difficult. A second intermediate path, based on results obtained for $NaAlH_4$ decomposition, has also been proposed [21]. The aluminium segregation at the surface of the particles [22,23] suggests that certain intermediate Al-species (AlH_3) could diffuse across the particle to release hydrogen. Despite AlH_3 has still not been detected, its decomposition temperature, between 70 and 150 °C [24], makes the process feasible.

On the other hand, milling treatment leads to a decomposition of $LiAlH_4$ ($LiAlH_4$ is metastable ($\Delta G^{\circ}_{r} < 0$) [20]). Balema et al. [11] have observed that $LiAlH_4$ decomposition occurs at long milling times. Balema suggests that impurities providing from milling enhance the decomposition of $LiAlH_4$ into Li_3AlH_6 and Al at long milling times. In fact, it has been reported that the presence of a great amount impurities reduce the thermodynamic stability of $LiAlH_4$ [25]. However, due to $LiAlH_4$ metastability, decomposition during milling could be also mechanically activated by the shocks during milling and/or by increasing vial temperature during milling treatment [26]. In first case, milling treatment could form new phases (for instance high pressure phases) [27,28] and subsequently, have an influence on the decomposition of $LiAlH_4$.

Balema et al. [11] have also been observed that milling improves the desorption H-kinetics of the $LiAlH_4$. Andreasen et al. [29] have recently attributed that enhancement to a reduction of crystallite size of $LiAlH_4$ which improves the species transport. However, the influence of parameters, such as particle size, vacancies density on H-kinetics has not been investigated yet and they may drastically affect to H-kinetics as occurs in other H-storage materials like MgH_2 [30].

The main purpose of this article is to clarify the thermal and mechanical decomposition mechanism of $LiAlH_4$ as well as the influence of parameters, such as particle size, crystallite size on its decomposition. To this aim, thermal analysis has been carried out to obtain the enthalpies and apparent activation energies of the decomposition reactions. Thermal measurements have been complimented by a structural and morphological characterisation by XRD, SEM and TEM in order to investigate the influence of particle and crystallite size on the decomposition process of $LiAlH_4$. Impurities providing for milling have been measured by ICP technique. Infrared spectroscopy (IR) has also been used to characterise the evolution of Al–H environment during mechanical milling.

2. Experimental

The starting material $LiAlH_4$ (>95%) was purchased from Sigma–Aldrich. The chemical synthesis of Li_3AlH_6 was performed according to the method described in literature [31]. To prevent any oxidation of samples and starting powders, all operations were carried out in an argon-atmosphere glove-box (<5 ppm O_2). As-received $LiAlH_4$ was milled inside the argon glove-box with a Fritsch P7 planetary mill. Milling was performed at a vial rotation speed of 230 rpm and with a ball to powder ratio of 10:1. Materials were milled for 30 min, 1.5, 7.3, 14, 35, and 70 h.

Elemental analysis of samples was done using an ICP-MS Perkin-Elmer Elan 6000. Samples were dissolved in concentrated HCl followed by the addition of distilled water. Then, they were analysed according to the normal procedure [32].

Structural analyses were done at room temperature by using a X-ray diffractometer Bruker D8 Advance equipped with Cu Kα radiation. Sample holders were filled inside the glove-box and covered with a Kapton foil to avoid any oxidation during the X-ray measurement. Diffraction patterns were analysed by the Rietveld method [33] using the Fullproff software.

The morphology of the samples was analysed by scanning electronic microscopy (SEM) with a Zeiss DSM 962, operating at 10 kV. Samples were transferred to the SEM under argon atmosphere by a glove bag. High-resolution transmission electron microscopy (HRTEM) analysis were performed on a JEOL 3000F FEG (point resolution 0.16 nm) operated at 300 kV. All operations have been carried out inside a nitrogen glove-box and the powders were dropped on an amorphous carbon-coated TEM copper grid by using hexane. $LiAlH_4$ was found to be stable under the electron beam.

Fourier transformation infrared (FT-IR) spectra were recorded with a Brucker Equinox 55 equipped with an attenuated total reflection (ATR) accessory. The spectral resolution was 4 cm^{-1}. Measurements were done under an argon atmosphere.

Thermal analyses were conducted with a DSC 404 C Pegasus from Netzsch. All measurements were carried out under a flow (50 ml/min) of high purity argon (99.999%). Sample mass was typically 10 mg. Heating runs were performed at different rates from 50 to 450 °C. Thermal desorption measurements (TDM) were performed with a home-made instrument under vacuum.

3. Results and discussion

3.1. Thermal decomposition of as-received $LiAlH_4$

As-received $LiAlH_4$ is formed of crystals with a well-defined monoclinic morphology as displayed in the SEM micrograph (Fig. 1). The crystals exhibit a bi-modal distribution in size centred around ~50 and ~150 μm. An average initial crystallite size greater than 300 nm is obtained by Rietveld method of X-ray diffraction pattern.

Fig. 2a–e shows the DSC curves of as-received $LiAlH_4$. Two different decomposition processes are observed depending on heating rate (HR). At HR above 1 °C/min, three peaks (I, II and III) are detected as shown Fig. 2a–c. Whereas endothermic peak I does not depend strongly on the HR, the position of endothermic peak II and exothermic peak III are shifted to lower temperatures when the HR is decreasing. Besides these peaks, a small exothermic peak is sometimes detected at ~150 °C [8,9] that is related to a reaction between $LiAlH_4$ and hydroxide traces present on the sample. Endothermic peak I does not depend on HR. During this process there is no hydrogen release as shown by

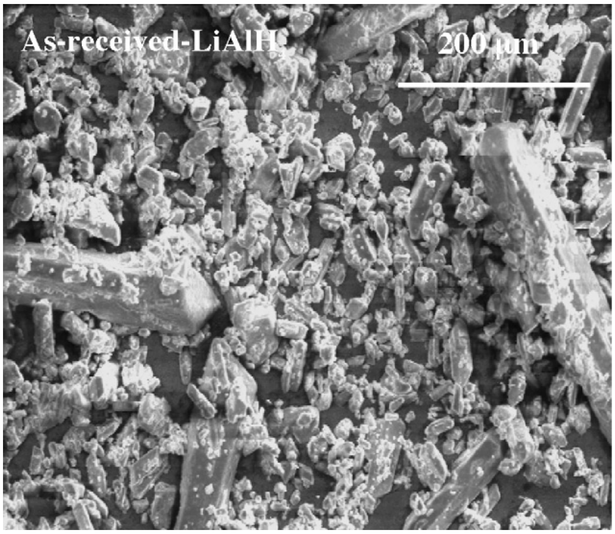

Fig. 1. SEM micrograph of as-received $LiAlH_4$.

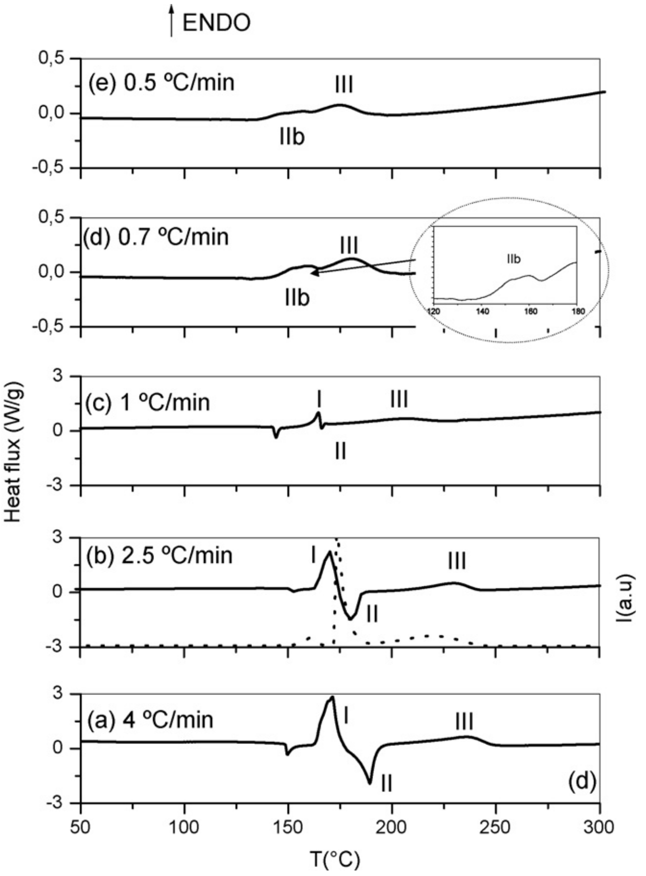

Fig. 2. (a–e) DSC curves of as-$LiAlH_4$ at different heating rates. The peaks of the reactions are marked. In (b), thermal desorption curve is shown with a dash line. Inset in (d) shows that step IIb is composed by two peaks.

TDM (Fig. 2b, dashed line) and the value obtained of reaction enthalpy (13 kJ/mol) corresponds to that of $LiAlH_4$(s) melting [10]. However, the exothermic peak II and the endothermic peak III exhibit a drastic dependence on HR. The relation of TDM peaks area is ~2 which confirms that peak II is associated with the decomposition of $LiAlH_4$(l) and the formation of solid Li_3AlH_6 with H_2 release (5.3 wt%) while peak III is related to the decomposition of Li_3AlH_6 into LiH with H_2 release (2.6 wt%). Reaction enthalpies obtained for the two peaks (−14 and 15 kJ/mol, respectively) are in agreement with data previously reported [9].

On the other hand, when HR is below 1 °C/min, only two endothermic peaks (IIb and III) are detected (Fig. 2d–e). The position of the peaks also depends on HR and no melting is detected. The process of melting and solidification has been substituted by an endothermic reaction (peak IIb) with an enthalpy of 1.6 kJ/mol. This value agrees with previously data obtained by computer calculations corresponding to the decomposition of $LiAlH_4$(s) into Li_3AlH_6(s) [34–36] and it is similar to an experimental data reported in Ref. [9]. As concern the higher temperature peak (III), the reaction exhibits a reaction enthalpy of 16 kJ/mol similar to that obtained at faster rates, which suggests that the same reaction occurs, i.e. decomposition of Li_3AlH_6 into LiH and Al without melting.

However, inset of Fig. 2d shows that peak IIb is double, which indicates that the decomposition reaction of $LiAlH_4$ exhibits intermediate stages. This stage may be related to induction or nucleation of a new phase (Li_3AlH_6 and Al) and the diffusion of some species, respectively [37] or due to intermediate reactions [38] (for instance, involving AlH_x species). Further investigation is necessary to clarify which processes occur during these stages.

The apparent activation energies, E_a, of the different processes were obtained by the non-isothermal Kissinger method [39]. Fig. 3 shows the E_a of the different reactions in a Kissinger plot. As concerns peaks II and IIb, i.e. decomposition of $LiAlH_4$ into Li_3AlH_6, the smaller apparent activation energy observed at higher heating rates (115 kJ/mol versus 162 kJ/mol) indicates that the release of hydrogen after melting is kinetically more favourable than

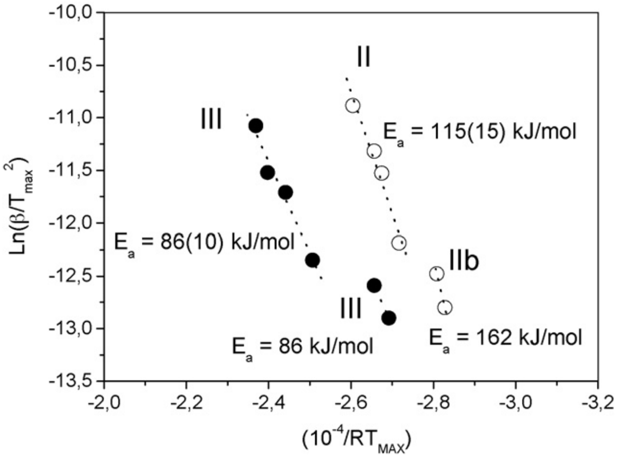

Fig. 3. Kissinger plot for the decomposition steps II, IIb and III. Heating rates varying from 0.5 to 4 °C/min. Apparent activation energies (E_a) of the reactions are given by the slope of the fittings of equation $\ln(\beta/T_{max}) = (-E_a/RT_{max}) + \text{constant}$ (T_{max} = peak temperature, β = heating rate, R = Boltzmann constant).

the release of hydrogen without melting. Melting suppression observed on decreasing HR is a phenomena observed with highly energetic materials [40] and it is explained by the ''near static conditions'' (slow HR) that allow a slow diffusion of species without melting, whereas higher HR leads to a more favourable reaction path which implies a melting of $LiAlH_4$ and, subsequently, a higher mobility of the atoms. These results may explain the decomposition of $LiAlH_4$ into Li_3AlH_6 below the melting point of $LiAlH_4$ as well as the discrepancies between results obtained from different techniques, such as NMR and XRD in situ analyses [18,19] and TG or DSC [10,17]. The value of E_a at lower HR (162 kJ/mol) is in good agreement to the value reported by Kang et al. [41] (154 kJ/mol). At faster heating rates, the obtained value of activation energy (115 kJ/mol) is slightly higher to this recently obtained by Blanchard et al. [37] (102 kJ/mol) and Andreasen et al. [29,42] (81 and 89 kJ/mol).

With regard to the higher temperature peak (III), i.e. decomposition of Li_3AlH_6 into LiH and Al without melting. The apparent activation energy exhibits a value of 86 kJ/mol as it is shown in Fig. 3 and it is not influenced by heating rate. This value is between the value reported (107 kJ/mol) by Andreasen et al. [29] and this given by Kang et al. (72 kJ/mol) [41].

3.2. Mechanically activated decomposition of as-$LiAlH_4$

Fig. 4 shows the thermal decomposition of $LiAlH_4$ milled for different times. Whereas $LiAlH_4$ milled for short times (≤14 h) releases hydrogen through the two basic reactions (Eqs. (1) and (2)) cited in Section 1, $LiAlH_4$ milled for longer times (>14 h) decomposes through one reaction (Eq. (2)). The evolution of the desorption temperature (T_d) and amount of hydrogen released for both reactions as a function of milling time are shown in Fig. 5a and b, respectively. Two stages are differentiated: at short milling time (<1.5 h) T_d of both decomposition reactions decreases by ~60 °C as well as the amount of hydrogen stored for the first reaction (~0.5 wt%). At intermediate milling time ($1.5\text{ h} < t < 14\text{ h}$) the temperature of both decomposition reactions remains constant and a slight hydrogen release is again observed (~0.5 wt%) for the first reaction. Further milling leads to $LiAlH_4$ decomposition into Li_3AlH_6 and Al.

3.2.1. Decomposition of as-received $LiAlH_4$ during milling

The influence of milling time on particle morphology of $LiAlH_4$ before decomposition is shown in the SEM micrographs displayed in Fig. 6a–c. For milling time below 1.5 h particles are refined. Whereas the sample milled 30 min shows still very large particles ($D_p = 80 \pm 40$ μm) that have not been completely milled, the sample milled 1.5 h exhibits already a finer and more homogeneous particle size distribution particle ($D_p = 30 \pm 15$ μm). At the end of this stage, smaller particles tend to agglomerate. Then, when increasing milling times (>1.5 h), as shown in Fig. 6c, $LiAlH_4$ particles agglomerate more and particle size is not further reduced ($D_p = 35 \pm 10$ μm).

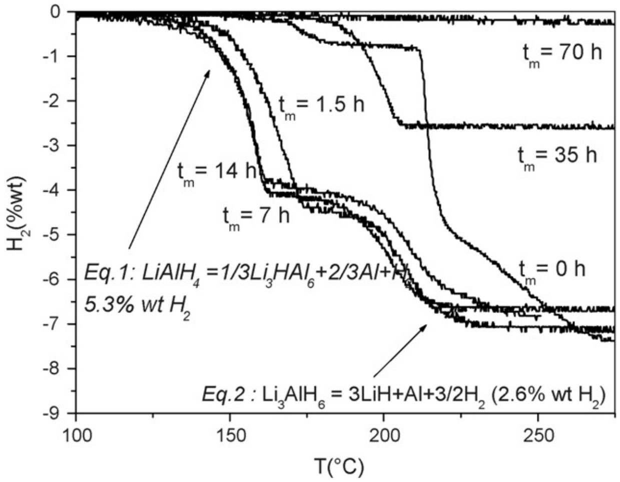

Fig. 4. Thermal desorption of $LiAlH_4$ milled different times. A heating rate of 8 °C/min was used.

To determine microstructural (crystallite size) and crystallographic properties (phase identification and cell volume) XRD patterns have been analysed by the Rietveld method. All patterns exhibit good refinements. Fig. 7a and b shows the XRD patterns of sample milled 1.5 and 7 h, respectively. All the peaks were indexed to a monoclinic $P2_1/c$ structure of $LiAlH_4$ but a small peak at 32.2° that corresponds to LiCl impurity. Table 1 shows that the crystallite size of $LiAlH_4$ decreases from initial values of 300 ± 50 to 90 ± 30 nm in only 30 min of milling and further milling time has no

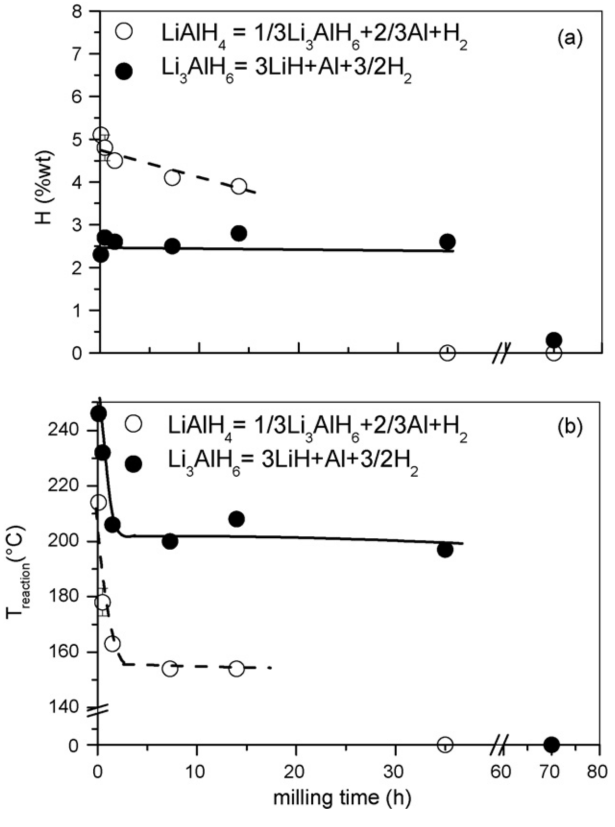

Fig. 5. (a) Influence of milling time on H-capacity of the two decomposition reactions. (b) Influence of milling time on temperatures of the two decomposition reactions.

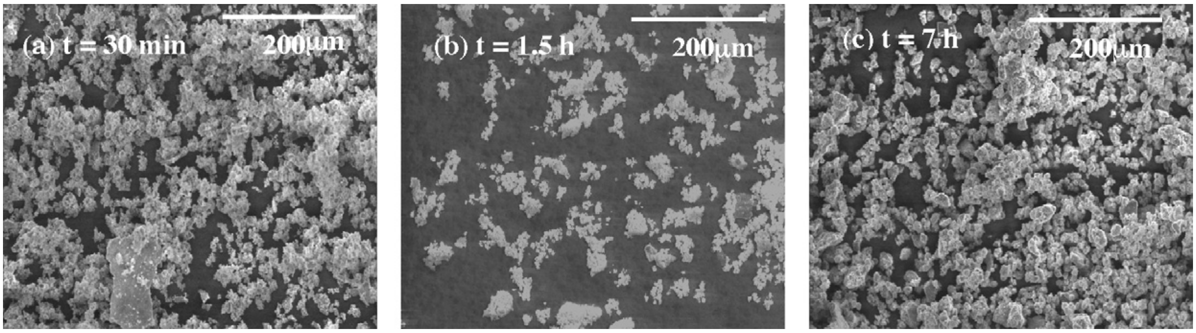

Fig. 6. SE micrographs (a) $LiAlH_4$ milled 30 min, (b) $LiAlH_4$ milled 1.5 h and (c) $LiAlH_4$ milled 7 h.

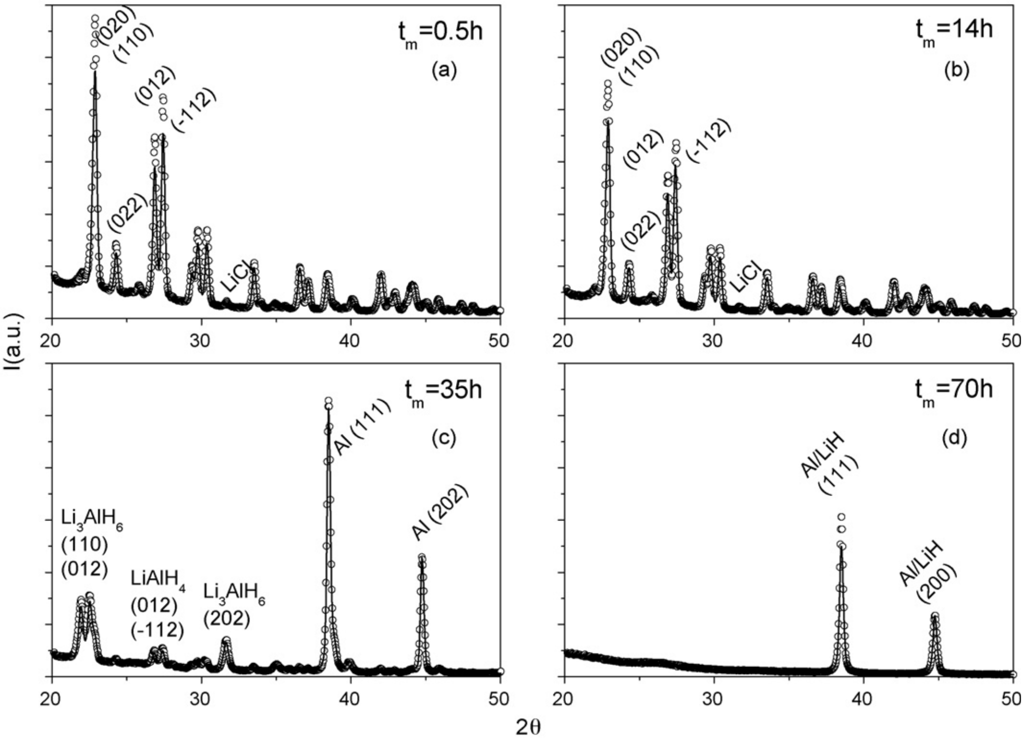

Fig. 7. XRD patterns of $LiAlH_4$ milled (a) 0.5, (b) 14, (c) 35 and (d) 70 h. The phases following phases were used to fit the patterns: monoclinic-$LiAlH_4$ ($P2_1/c$), rombohedric-Li_3AlH_6 (R-3), cubic-LiH (Fm-3m) and cubic-Al (Fm-3m). The continuous line is the fit. More intense peaks are marked. The quality of the refinement is given by the weight profile factor (R_{wp}). All patterns exhibit $9\% < R_{wp} < 14\%$.

Table 1
Values of crystallite size and cell volume of $LiAlH_4$ phase milled different times

$LiAlH_4$, t_{milled} (h)	D_v (nm)	V_{cell} (Å^3)
0	300 (50)	277.2 (1)
0.5	91 (30)	277.1 (1)
1.5	90 (20)	277.1(1)
7	130 (30)	277.0 (1)
14	109 (40)	276.6 (1)

Values are obtained by Rietveld analyses of the diffraction patterns.

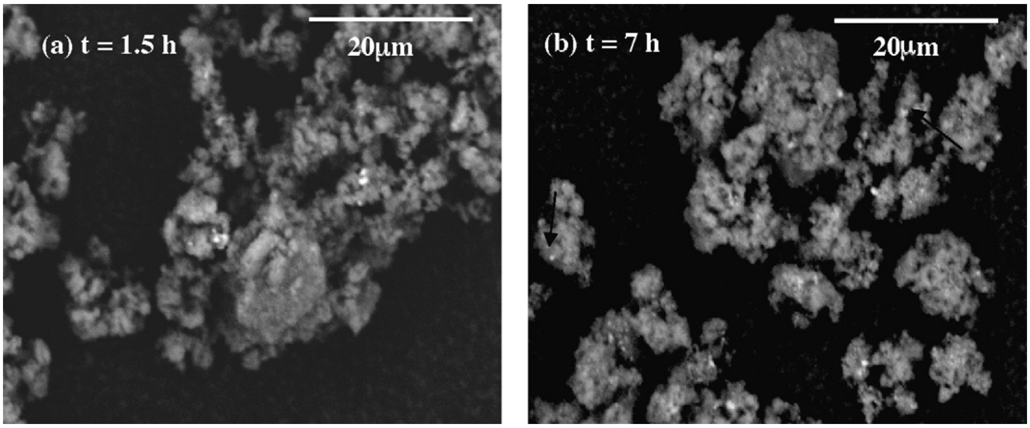

Fig. 8. Backscattering micrographs of $LiAlH_4$ milled (a) 1.5 and (b) 7 h. White dots correspond to Al.

influence on crystallite size. As concerns crystallographic properties, the cell volume of $LiAlH_4$ is not drastically affected by milling treatment.

Although $LiAlH_4$ is the only phase detected in the X-ray diffraction pattern, Figs. 4 and 5 show that $LiAlH_4$ milled for 1.5 h exhibits a slight diminution of H-capacity (0.5 wt%) compared to as-received $LiAlH_4$ which suggests that decomposition of $LiAlH_4$ has already taken place. In fact, a small amount of Al is detected by BSE at the surface of $LiAlH_4$ particles, as displayed in Fig. 8a. This confirms that $LiAlH_4$ is partially decomposed after 1.5 h of milling. When milling time is increased up to 7.5 h, the amount of stored hydrogen for the first reaction is further decreased (by 1 wt%) compared to as-received $LiAlH_4$ (Fig. 5a). As a consequence, a higher amount of Al at the particle surface is observed in the corresponding BSE micrograph (Fig. 8b). Therefore, the decomposition of $LiAlH_4$ occurs at very short milling times. So, because the amount of impurities detected by ICP is negligible and the vial temperature during milling (~50 °C) is lower than decomposition temperature of $LiAlH_4$, decomposition of $LiAlH_4$ is rather related to the high pressures and temperature rise locally created during milling than thermal decomposition by increasing the temperature of vial or impurities generated during milling.

Moreover, Fig. 9a shows the selected area electron diffraction (SAD) pattern of one particle of $LiAlH_4$ milled 1.5 h. The particle is mainly composed of nanocrystalline $LiAlH_4$. However, in a HRTEM image of the particle (Fig. 9b), besides the planes corresponding to $LiAlH_4$ monoclinic phase, several planes within the crystalline part of the particle can be indexed by a different phase. These planes may be indexed to the tetragonal high-pressure phase Li_3AlH_6 [43]. Formation of high-temperature–pressure metastable phases are commonly occurring during milling [44] and it has been observed with other ionic hydrides, such as MgH_2 [45]. However, with regard to high pressure Li_3AlH_6, the actual lack of crystallographic and thermodynamical data [27] as well as its low quantity make complicated to discern whether this phase is a intermediate stage during the decomposition reaction or simply the result of milling the normal pressure phase Li_3AlH_6. Nevertheless, the local presence of the high-pressure phase suggests that the decomposition is driven mechanically.

At longer milling times (35 h), the total decomposition of $LiAlH_4$ is almost achieved. Fig. 7c shows the pattern diffraction of the sample milled 35 h. Two new phases were found: Li_3AlH_6 indexed to a rhombohedral *R*-3 [46] and Al, indexed to a cubic *Fm-3m*. Also, a small quantity of $LiAlH_4$ phase is detected. With regard to microstructure, large crystallite size values (~80 nm) of both phases are obtained by Rietveld analysis. Further milling (up to 70 h) leads to the full decomposition of Li_3AlH_6 into LiH and Al as shown in Fig. 7d.

Fig. 10a shows the morphology of the sample milled 35 h in a SEM micrograph. After decomposition, particle size distribution is roughly similar to that before decomposition. The particles exhibit a more homogeneous shape as a result of the phase transformation. BSE micrograph of the sample is shown in Fig. 10b. Particle exhibits large amount of aluminium on the surface that confirms that decomposition took place. Aluminium at the surface of the particles has recently been detected during the thermal decomposition of $LiAlH_4$ [22], which suggests similarities between thermal and mechanical decomposition as well as the existence of a long-range transport mechanism of Al species during mechanical decomposition. SAD measurements in Fig. 11a confirm that particles milled 35 h are formed by a rhombohedral Li_3AlH_6 and Al. Moreover, a small layer (~5 nm) is detected on the surface by HRTEM as shown

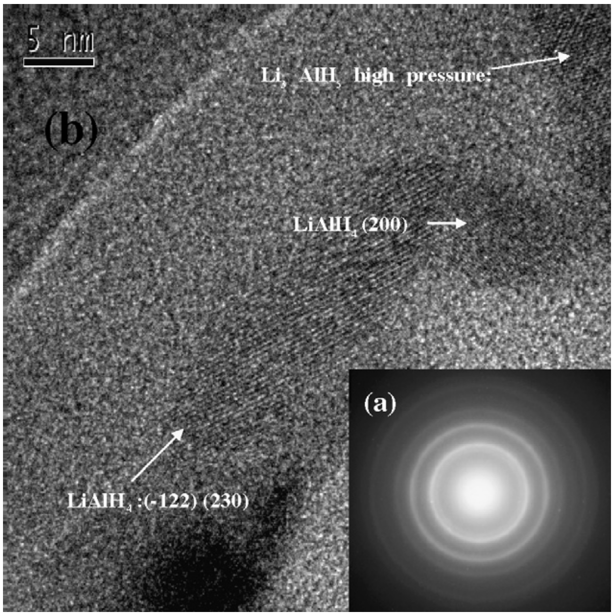

Fig. 9. (a) SAD of a particle after milled 1.5 h. (b) HRTEM image showing lattice.

Fig. 11b. This layer was only observed on particles milled for 35 h, which indicate that is formed after the decomposition of $LiAlH_4$ into Li_3AlH_6 and Al. Besides, measurements of EDS in the particles reveal a higher ratio O/Al into this layer than inside of the particle. Therefore, due to the large quantity of aluminium observed on the surface, the surface layer could be due to the oxidation of aluminium from decomposition reaction. In fact, after milling process, sample becomes more active due to larger surface/volume of the particles and oxygen could have been introduced either during milling or handling the sample. A similar oxide layer was found by Andrei et al. [22] in $LiAlD_4$ milled with different additives. Although the role of this layer is beyond of the scope of this paper, it is feasible to expect some influence of this layer on the decomposition processes of the alanate, such as species diffusion, H-surface dissociation, etc.

The decomposition process of $LiAlH_4$ was also followed by IR spectroscopy. Recently, this technique has been used in as-received $NaAlH_4$ and milled $NaAlH_4$ [47]. In $LiAlH_4$, AlH_4^- ion has a tetrahedral symmetry with active infrared frequencies in two regions [48] Al–H stretching modes ν_3(F2) at 1600–1800 cm^{-1} and Li–Al–H bending modes, ν_4(F2) at 700–900 cm^{-1}. Nevertheless, due to a slight distortion in the solid state (AlH_4^- ions having a

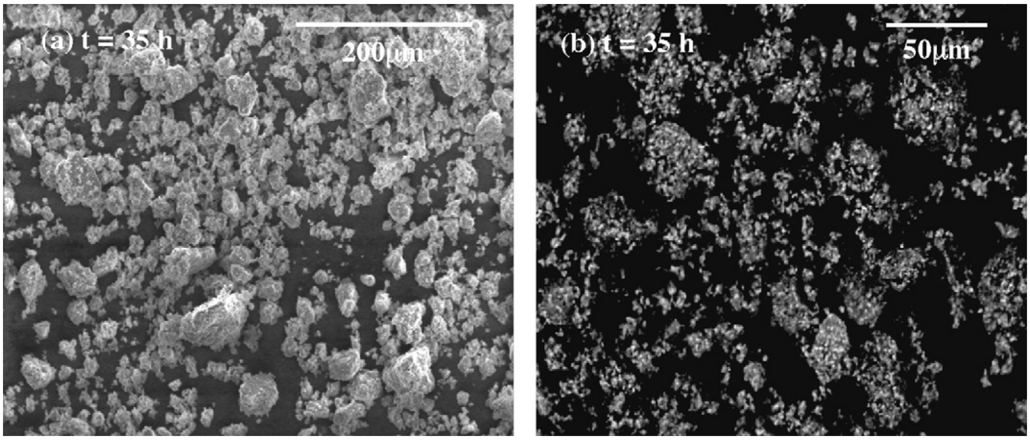

Fig. 10. (a) SE and (b) backscattering micrographs of $LiAlH_4$ milled 35 h. White dots correspond to Al.

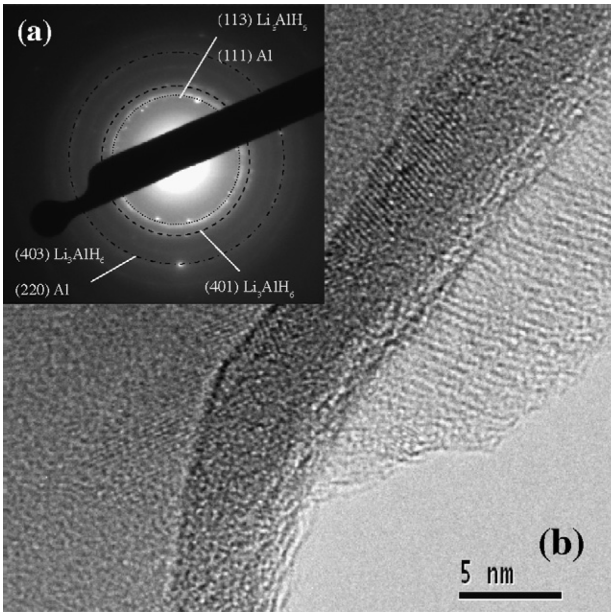

Fig. 11. (a) SAD of $LiAlH_4$ particle after 35 h of milling. (b) HRTEM image of one particle. An oxide layer is observed on surface.

flattened tetrahedral symmetry (D_{2d})), a splitting of the active bands in infrared is usually observed [49–52]. Fig. 12i shows the IR spectrum of as-received $LiAlH_4$. The bands observed correspond to the one previously reported [50,51] for solid $LiAlH_4$ with stretching modes at 1760 and 1610 cm^{-1} and bending modes at 900 and 803 cm^{-1}.

As concerns to Li_3AlH_6, solid Li_3AlH_6 has been synthesised according to the method described in [31] for comparative purposes. $[AlH_6]^{3-}$ has an octahedral symmetry and shows active infrared frequencies around [50]: 1400 cm^{-1} for the stretching mode ν_3(F1) and 990 cm^{-1} for the bending mode ν_4(F1). The IR spectrum of Li_3AlH_6 is

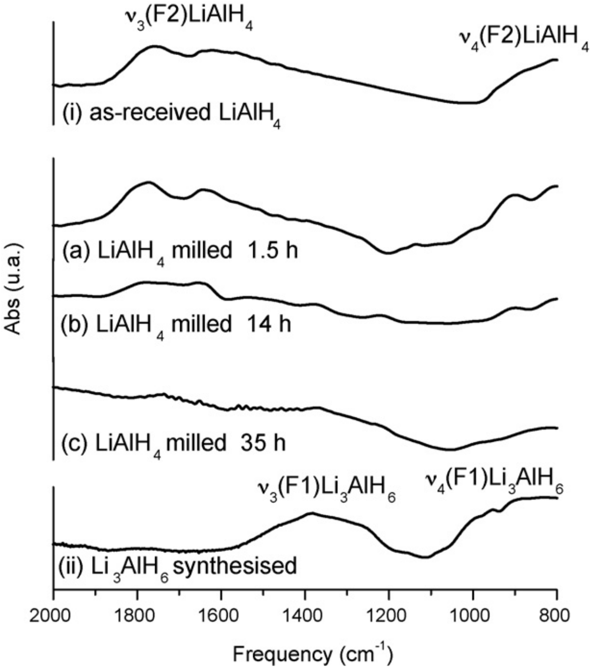

Fig. 12. IR spectrum of (i) as-received $LiAlH_4$, (ii) Li_3AlH_6 synthesised, (a) $LiAlH_4$ milled 1.5 h, (b) $LiAlH_4$ milled 14 h and (c) $LiAlH_4$ milled 35 h.

presented Fig. 12ii. The bands observed at 1390 and 1250 cm^{-1} for the stretching modes and 1000, 950 cm^{-1} for the bending modes are in agreement with the ones reported by Bureau et al. [51].

When $LiAlH_4$ is milled for a short time, a small shift (20 cm^{-1}) to high frequencies of the stretching modes is observed (Fig. 12a). This shift may be related to the strain created during milling because a similar shift was observed [28] by Raman spectroscopy for $LiAlH_4$ under a static pressure (~5 GPa) similar to the one expected during mechanical milling. Further milling (Fig. 12b and c) leads to a decrease in $LiAlH_4$ peaks intensity until they disappear and two new bands at 1375 and at 1220 cm^{-1} are detected. Despite intensities are not very strong, their positions are similar to those of Li_3AlH_6 synthesised [52] that confirmed the near total decomposition of $LiAlH_4$ into Li_3AlH_6 during mechanical milling. Decomposition occurs without intermediate products detected by IR measures.

3.2.2. Thermal decomposition of milled $LiAlH_4$

The evolution of the desorption temperature (T_d) and amount of hydrogen released for both reactions as function of milling time have been shown in Fig. 5a. At short milling times (<1.5 h) T_d of both decomposition reactions decreases by ~60 °C whereas at intermediate milling times (1.5 h $< t <$ 14 h) the temperature of both decomposition reactions remains constant. Further milling lead to $LiAlH_4$ decomposition as shown in Section 2.

Temperature reduction of both decomposition reactions could be facilitated by reduction of particle and crystallite size and, in certain cases by defects and impurities introduced during milling. As concerns impurities, it has been reported that impurities uptakes could act as a catalyst for the decomposition of $LiAlH_4$ [11]. However, the amount of impurities detected by ICP after milling $LiAlH_4$ for 70 h is much lower (<0.1 wt% of iron impurity) than those reported in literature [12,13]. Therefore, the amount of impurities arising from milling tools is not the main cause of the diminution of T_d. A higher vacancy density could also contribute in reducing the desorption temperatures as suggested by Fitchtner et al. [53]. Nevertheless, in our case, structural parameter as cell volume stays practically constant during milling as it was shown in Table 1. With regard to microstructure, a crystallite size remains constant after 30 min of milling but temperature continues decreasing up to longer milling times. Thus, reduction of crystallite size is not the main reason to explain the temperature reduction of both reactions. However, Fig. 6a and b shows that $LiAlH_4$ milled 30 min still has very big particles compared to the same sample milled 1.5 h, which exhibits a finer and more homogeneous particle size distribution. Hence, a influence on T_d is expected, i.e. smaller particles exhibit shorter diffusion paths and then, decomposition temperature is lower than those with larger ones. Further milling leads (>1.5 h) to agglomeration of the particles as shown Fig. 6c, and not further particle size refinement is observed. Therefore, the temperature of both reactions remains constant, as shown Fig. 5b, suggesting that particle size controls the decomposition temperature of both reactions.

Moreover, milling $LiAlH_4$ for short times has an influence on its thermal decomposition mechanism. Fig. 13 shows the DSC curve of $LiAlH_4$ milled 1.5 h. No melting was detected and two endothermic peaks similar to those observed for as-received $LiAlH_4$ were observed. These peaks exhibit also similar reaction enthalpies: 1.8 and 20 kJ/mol

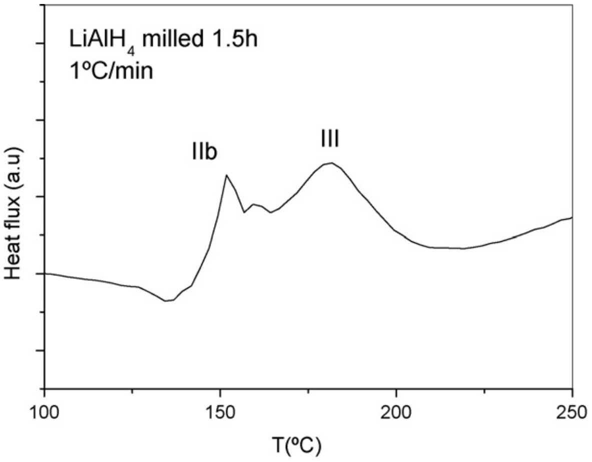

Fig. 13. DSC curve of $LiAlH_4$ milled 1.5 h.

suggesting similar thermal decomposition processes to those observed in the decomposition of as-received $LiAlH_4$ at lower heating rates.

The activation energies of the two decomposition reactions of milled $LiAlH_4$ ($t = 1.5$ h) were calculated by Kissinger method. An activation energy of 100 ± 10 kJ/mol was obtained in the first decomposition reactions and a 130 ± 15 kJ/mol in the second decomposition reaction. Therefore, the activation energy of the first decomposition reaction of milled $LiAlH_4$ is smaller than this of as-received $LiAlH_4$. The difference could be related to the diminution of crystallite size produced by milling during the first 30 min. A smaller crystallite size would improve the decomposition kinetics and it would reduce the activation energy. However, with regard to the second reaction, an increase of the activation energy as compared to un-milled sample is found. This may be attributed to the influence of aluminium oxides (previously detected by TEM) and/or high-pressure phases that could degrade the process of decomposition of Li_3AlH_6.

4. Conclusions

The mechanism of thermal decomposition of $LiAlH_4$ depends on HR. Whereas slow HR lead to an endothermic decomposition of $LiAlH_4$ into Li_3AlH_6 without melting and with intermediate processes, fast HR lead to melting before decomposition of $LiAlH_4$ into Li_3AlH_6 and diminution of the apparent activation energy. However, the apparent activation energy of the subsequent decomposition of Li_3AlH_6 into LiH and Al does not depend on HR. Mechanical milling of $LiAlH_4$ leads to its decomposition into Li_3AlH_6 and Al, and after, Li_3AlH_6 decomposes of into LiH. The process of decomposition is mechanically driven and Aluminium is detected at particle surface (during milling of $LiAlH_4$) suggesting the existence of a long-range transport mechanism of Al-species during mechanical decomposition. Besides, HTREM measurements reveal the existence of an oxide layer on the surface of the alanate and a formation of high-pressure phase due to milling treatment. Finally, milling $LiAlH_4$ results in reduction of both temperature reactions. This reduction is mainly attributed to shorter diffusion paths because of a diminution of particle size during the milling treatment.

References

[1] B.A.M. Seayal, D.M. Antobelli, Adv. Mater 16 (2004) 9.
[2] L. Schlapbach, A. Züttel, Nature 414 (2001) 353.
[3] B. Bogdanovic, M. Schwickardi, J. Alloys Compd. 253/254 (1997) 1.
[4] G.J. Thomas, K.J. Gross, N.Y.C. Yang, C. Jensen, J. Alloys Compd. 330–332 (2002) 702.
[5] B. Bogdanovic, R.A. Brand, A. Marjanovic, M. Schwickardi, J. Tolle, J. Alloys Compd. 302 (2000) 36.
[6] D. Sun, T. Kiyobayashi, H.T. Takeshita, N. Kuriyana, C.M. Jensen, J. Alloys Compd. 337 (2002) L8.
[7] N. Sklar, B. Post, Inorg. Chem. 6 (1967) 669.
[8] M. McCarty, J.N. Maycock, V.R. Pai Verneker, J. Phys. Chem. 72 (12) (1968) 4009.
[9] P. Claudy, B. Bonnetot, J.M. Letoffe, G. Turck, Thermochim. Acta 27 (1978) 213.
[10] J.P. Bastide, B. Bonnetot, J.M. Letoffe, P. Claudy, Mater. Res. Bull. 20 (1985) 999.
[11] V.P. Balema, V.K. Pecharski, K.W. Dennis, J. Alloys Compd. 313 (2000) 69.
[12] V.P. Balema, J.W. Wiench, K.W. Dennis, M. Pruski, V.K. Pecharski, J. Alloys Compd. 1/2 (329) (2001) 108.
[13] M. Resan, H.D. Hampton, J.K. Lomness, D.K. Slattery, Int. J. Hydrogen Energy 30 (13/14) (2005) 1413.
[14] M. Resan, H.D. Hampton, J.K. Lomness, D.K. Slattery, Int. J. Hydrogen Energy 30 (13/14) (2005) 1417.
[15] J. Chen, N. Kuriyama, Q. Xu, H.T. Takeshita, T. Sakai, J. Phys. Chem. B 105 (2001) 11214.
[16] J.A. Dilts, E.C. Ashby, Inorg. Chem. 116 (6) (1972) 1230.
[17] T.N. Dymova, V.N. Konoplev, D.P. Aleksandrov, A.S. Sizareva, T.A. Silina, Russ. J. Coord. Chem. 21 (3) (1995) 165.
[18] H.W. Brinks, B.C. Hauback, P. Norby, H. Fjellvag, J. Alloys Compd. 351 (2003) 222.
[19] J.W. Wiench, V.P. Balema, V.K. Percharski, M. Pruski, J. Solid State Chem. 177 (3) (2004) 648.
[20] T.N. Dymova, D.P. Aleksandrov, V.P. Konoplev, T.A. Silina, N.T. Kuznetsov, Russ. J. Coord. Chem. 19 (1993) 607.
[21] K.J. Gross, S. Guthrie, S. Takura, G. Thomas, J. Alloys Compd. 297 (2000) 270.
[22] C.M. Andrei, J.C. Walmsley, H.W. Brinks, R. Holmestad, D. Blanchard, B.C. Hauback, G.A. Botton, J. Phys. Chem. B 109 (2005) 4350.
[23] C.M. Andrei, J.C. Walmsley, D. Blanchard, H.W. Brinks, R. Holmestad, B.C. Hauback, J. Alloys Compd. 395 (1/2) (2005) 307.
[24] G. Sandrock, J. Reilly, J. Graetz, W.-M. Zhou, J. Johnson, J. Wegrzyn, Appl. Phys. A 80 (2005) 687.
[25] N.N. Mattesva, A.I. Golanova, Russ. J. Appl. Chem. 73 (2000) 747.
[26] D.S. Easton, J.H. Scheinbel, S.A. Speakman, J. Alloys Compd. 398 (2005) 135.
[27] P. Vajeeston, P. Ravindran, A. Kjekshus, H. Fjellvag, Phys. Rev. B 69 (2004) 020104.
[28] A.V. Talyzin, B. Sundqvist, Phys. Rev. B 70 (2004) 180101.

[29] A. Andreasen, T. Vegge, A.S. Pedersen, J. Solid State Chem. 178 (2005) 3664.
[30] F.-K. Aguey-Zinzou, J.R. Ares, T. Klassen, R. Bormann, Mater. Res. Bull. 41 (2006) 1118.
[31] J. Mayet, S. Kovacevicard, J. Tranchant, Bull. Soc. Chim. 2 (42) (1973) 503.
[32] S.J. Hill, Inductively Coupled Plasma Spectrometry and its Applications, Sheffield Academic Press, UK, 1999.
[33] J. Rodriguez-Carvajal, Physica B 192 (1993) 55.
[34] S.-C. Chung, H. Morioka, J. Alloys Compd. 372 (2004) 92.
[35] O.M. Lovvik, S.M. Opalka, H.W. Brinks, B. Hauback, Phys. Rev. B 69 (2004) 134117.
[36] T.J. Frankcombe, G.-J. Kroes, Chem. Phys. Lett. 423 (1–3) (2006) 102–105.
[37] D. Blanchard, H.W. Brinks, B.C. Hauback, P. Norby, J. Muller, J. Alloys Compd. 404–406 (2005) 743.
[38] R.T. Walters, J.H. Scogin, J. Alloys Compd. 421 (1-2) (2006) 54–56.
[39] H.E. Kissinger, Anal. Chem. 29 (1958) 1702.
[40] Th. Rieckman, S. Völker, L. Lichtblan, R. Schirra, J. Anal. Appl. Pyrolysis 58/59 (2001) 569.
[41] J.K. Kang, J.K. Lee, R.P. Muller, W.A. Goddard, J. Chem. Phys. 121 (21) (2004) 10623.
[42] A. Andreasen, J. Alloys Compd. 419 (1/2) (2006) 40.
[43] S. Konovalov, B. Bolychev, V. Genchel, Russ. J. Inorg. Chem. (Engl. Trasl.) 35 (1990) 327.
[44] C. Surynarayara, C. Prog. Mater. Sci. 41 (2001) 1.
[45] J. Huot, G. Liang, S. Boily, A. Van Neste, R. Shultz, J. Alloys Compd. 293–295 (1999) 495.
[46] H.W. Brinks, B.C. Hauback, J. Alloys Compd. 354 (2003) 143.
[47] S. Gomes, G. Renardin, H. Hagermann, K. Yvon, M.P. Sulic, C.M. Jensen, J. Alloys Compd. 390 (2002) 305.
[48] K. Nakamoto, Infrared and Raman Spectra of Inorganic and Coordinated Compounds, Part A, fifth ed., J. Wiley, 1997,, p. 189.
[49] A.E. Shirk, F. Shriver, J. Am. Chem. Soc. 95 (18) (1973) 5904.
[50] B.M. Bulychev, V.N. Verbetskii, K.V. Semenenko, Russ. J. Inorg. Chem. 22 (11) (1977) 1611.
[51] J.C. Bureau, B. Bonnetot, P. Claudy, H. Eddaoudi, Mater. Res. Bull. 20 (1985) 1147.
[52] J.C. Bureau, Z. Amri, P. Claudy, J.M. Letoffe, Mater. Res. Bull. 24 (1989) 23.
[53] M. Fichtner, P. Canton, O. Kircher, A. Leon, J. Alloys Compd. 404–406 (2005) 732.